Macromolecular Bioscience
www.mbs-journal.de

The Effect of Ligand Mobility on the Cellular Interaction of Multivalent Nanoparticles

*Sara Maslanka Figueroa, Daniel Fleischmann, Sebastian Beck, and Achim Goepferich**

Multivalent nanoparticle binding to cells can be of picomolar avidity making such interactions almost as intense as those seen with antibodies. However, reducing nanoparticle design exclusively to avidity optimization by the choice of ligand and its surface density does not sufficiently account for controlling and understanding cell–particle interactions. Cell uptake, for example, is of paramount significance for a plethora of biomedical applications and does not exclusively depend on the intensity of multivalency. In this study, it is shown that the mobility of ligands tethered to particle surfaces has a substantial impact on particle fate upon binding. Nanoparticles carrying angiotensin-II tethered to highly mobile 5 kDa long poly(ethylene glycol) (PEG) chains separated by ligand-free 2 kDa short PEG chains show a superior accumulation in angiotensin-II receptor type 1 positive cells. In contrast, when ligand mobility is constrained by densely packing the nanoparticle surface with 5 kDa PEG chains only, cell uptake decreases by 50%. Remarkably, irrespective of ligand mobility and density both particle types have similar EC50 values in the 1–3 × 10^{-9} M range. These findings demonstrate that ligand mobility on the nanoparticle corona is an indispensable attribute to be considered in particle design to achieve optimal cell uptake via multivalent interactions.

1. Introduction

Nanoparticles (NPs) are considered ideal candidates for drug delivery because they are able to convey their cargo to a desired site of action, thus avoiding the deleterious consequences of off-target effects.[1] To achieve specific NP–cell interactions, particle surfaces are usually functionalized with ligands that are able to recognize distinct cellular structures. To counterbalance the affinity loss derived from the tethering of ligands to linkers,[2] numerous ligand molecules are coupled to a single NP to enable the simultaneous recognition of several receptor molecules on the cell membrane. This multivalent binding highly increases the nanomaterial's overall avidity,[3] which is why over the last years the research focus has been set on improving this trait. Still, targeted nanomaterials fail to achieve optimal results and studies deliver highly variable outcomes. This can mainly be attributed to an incomplete understanding of the influence that distinct particle design features have on multivalent interactions and, therefore, the particle's fate after binding. Additionally, adjustment of one particle attribute usually correlates with modifications of several other characteristics, which highly influences the outcome at cellular level. Therefore, a profound understanding of the parameters affecting multivalent binding is needed to improve NP design.

There are several factors that are known to influence a nanomaterial's multivalent binding, and thus the targeting capacity of NPs, such as particle size and receptor- or ligand density.[4,5] The latter not only determines the ability of a NP to bind to the target cell surface, but also the thermodynamic feasibility of cellular uptake[6] and its precise pathway.[7] Still, there are several other elements that contribute to the thermodynamic favorability of a multivalent interaction, among which flexibility was noted to be crucial by several publications.[8,9] In their seminal theoretical paper, Kitov and Bundle highlight that the flexibility of a system significantly increases the number of ways in which bonds can be formed in a multivalent interaction which, in turn, supports binding.[10] More so, they predict the compensation of the entropy loss derived from a binding by an increase in possible conformations and a reduced steric burden.[10] Therefore, a higher flexibility in a particle system that allows for a higher ligand mobility could enhance cellular interaction. However, ligand mobility on the particle corona is not sufficiently taken into consideration in particle design. Furthermore, the interplay between ligand mobility and ligand density is not yet completely understood.

NPs are commonly shielded by polymers, such as poly(ethylene glycol) (PEG), which, beside acting as a tether for ligands, enable prolonged circulation times[11] and reduce plasma protein absorption.[12] To achieve those effects, a high polymer surface density is usually required,[13] which restrains the flexibility of the system and the ligand mobility. Generally, the polymers comprising the NP corona are kept homogeneous in terms of length, i.e., molecular weight, and the multivalent interactions are to some extent length-dependent.[14] For

S. Maslanka Figueroa, D. Fleischmann, S. Beck, Prof. A. Goepferich
Department of Pharmaceutical Technology
University of Regensburg
Regensburg, Universitaetsstrasse 31 93053, Germany
E-mail: achim.goepferich@ur.de

The ORCID identification number(s) for the author(s) of this article can be found under https://doi.org/10.1002/mabi.201900427.

DOI: 10.1002/mabi.201900427

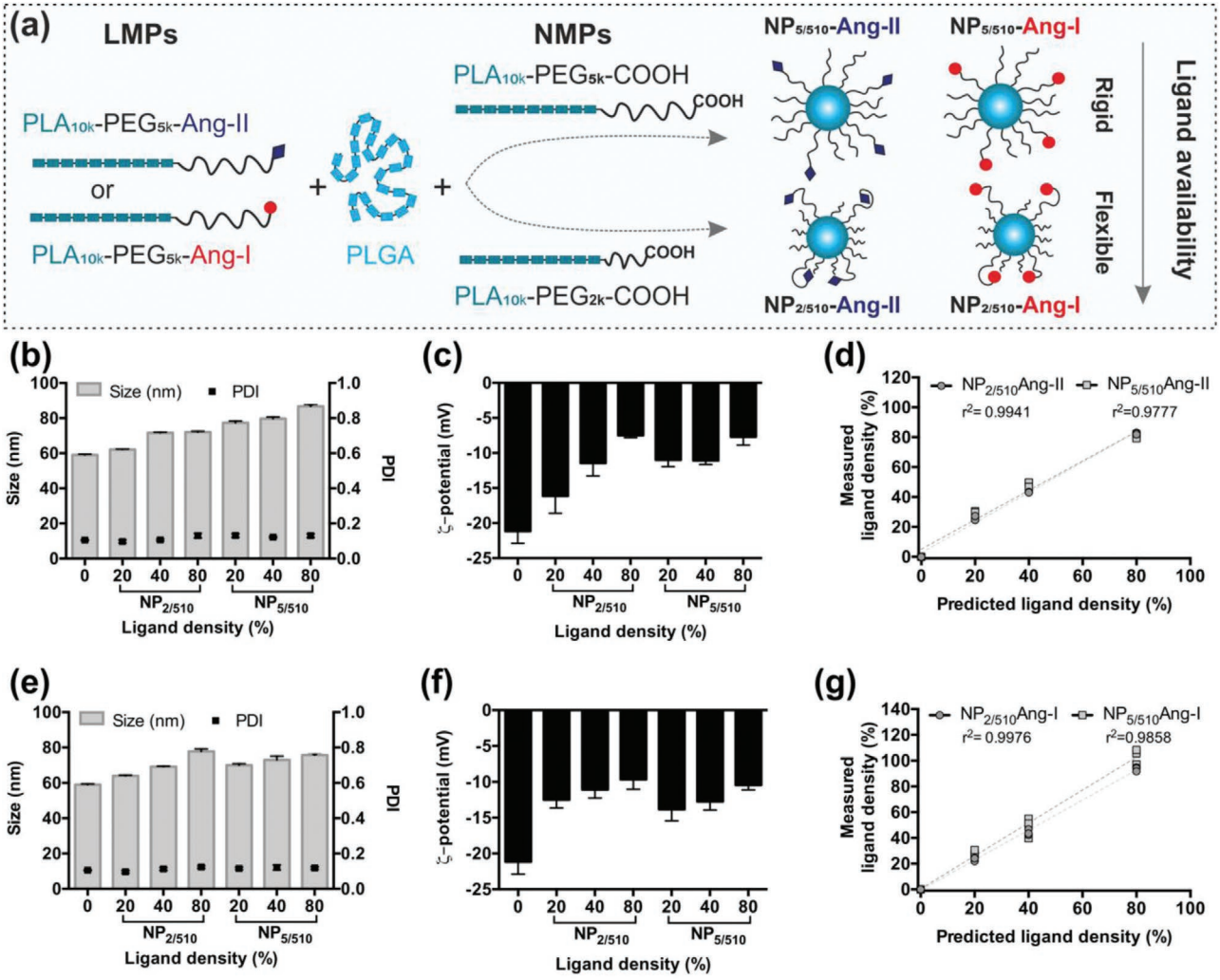

Figure 1. Composition a) and characterization of Ang-II b–d) and Ang-I e–g) targeted NP formulations. Hydrodynamic diameter measured by DLS b,e), ξ-potential c,f), and correlation of the measured normalized molar ligand content and the predicted ligand density d,g). Results are presented as mean ± SD of at least $n = 3$ measurements.

example, it was demonstrated that decreasing the overall PEG length can increase the uptake of liposomes[15] and polymer NPs.[16] However, these adjustments in polymer composition can reduce the overall particle PEG covering. Concomitantly, they tremendously alter particle size, which is a key factor determining NP–cell interactions,[17] making it difficult to discern which parameter contributed to the targeting increase. Therefore, the goal of this study was to investigate the effect of ligand mobility while maintaining a high PEG density and producing minor particle size variations. For our purposes we decided to design NPs with heterogeneous surface polymer compositions, a design choice sparsely represented in the literature.[15,18–21] To date, this concept is loosely associated with higher targeting efficiency or improved ligand binding and density control, but a deeper understanding of how it affects ligand mobility is required.

For our systematic investigation on the impact of ligand mobility on multivalent targeting particles, we relied on polymer NPs as a scaffold, consisting of PEG-poly(lactic acid)(PLA) and poly(lactic-co-glycolic acid) (PLGA). We considered them highly suited for this study as their ligand mobility can be tailored by adjusting the polymer composition. More so, they are biocompatible and biodegradable and are fitted for the use as drug carriers. To endow particles with targeting capacities we used angiotensin derivative ligands, which we previously used for highly specific cell identification,[22] and sought to further improve the system by adjusting its flexibility. To that end, we coupled angiotensin-I (Ang-I) or angiotensin-II (Ang-II), targeting cell membrane-bound angiotensin converting enzyme (ACE) or angiotensin-II type 1 receptor (AT1R), respectively, to long PEG_{5k}-PLA_{10k} chains and kept the remaining nonmodified polymers (NMPs) shorter by using a PEG_{2k}–PLA_{10k} to allow higher conformational freedom to the ligand-carrying polymers (LMPs) (**Figure 1**a). We compared this "flexible" NP-design with particles carrying NMPs of the same length as the LMPs, representing the conventional NP formulations. Additionally, we manufactured particles with increasing ligand densities to investigate if higher targeting capability (more ligands) would compensate for the associated mobility loss. The resulting NP formulations were characterized

in terms of size, surface charge, and ligand content. Their ligand affinity and particle avidity toward their respective targets were evaluated, and their cellular interaction regarding targeting efficiency, uptake specificity, and cellular distribution was analyzed. Finally, the polymer conformation on the particle corona and the distance between ligands was estimated.

2. Results and Discussion

2.1. Ligand Decorated NPs

To study the effect of ligand mobility on the NP–cell interactions, we chose polymeric PEG–PLA NPs with a PLGA-stabilized hydrophobic core, to avoid size increases resulting from a stabilization with high molecular weight PLA.[23] Such NPs are well-known for their biocompatibility and high versatility, as the particle composition can be precisely tailored by combining different PEG–PLA block copolymers (Figure 1a). Additionally, they are readily prepared via bulk nanoprecipitation of organic polymer solutions in aqueous medium. We covalently coupled ligands to longer carboxylic acid-terminated PEG_{5k}–PLA_{10k} copolymers prior to NP preparation (Figure S1, Supporting Information), which allows for precise control of the ligand density on the NP corona. NMPs were either the same length as the LMPs with carboxylic acid-ended PEG_{5k}–PLA_{10k} (COOH–PEG_{5k}–PLA_{10k}) or a shorter COOH–PEG_{2k}–PLA_{10k} to create NPs with homo- or heterogeneous polymer shells ($NP_{5/510}$ or $NP_{2/510}$, respectively) with varying ligand densities (Figure S2, Supporting Information). To impart specific recognition ability to our NPs, we chose to use two peptidic ligands that target a receptor and/or a cell membrane-bound enzyme, Ang-II and Ang-I, respectively. Ang-II is known for its high-affinity to the AT1R,[24] which upon binding is responsible for receptor-mediated endocytosis.[25] Ang-I is a substrate for ACE,[26] which we recently used to develop highly specific virus-mimetic NPs.[22] The binding of Ang-I-decorated NPs to the cell membrane-bound ACE results in the excision of the last two amino acids of the peptide, generating Ang-II-carrying NPs that are internalized through AT1R-mediated endocytosis. To minimize any possible interference on the NP–cell interaction,[27] the polymers were chosen to keep the particles in a narrow size range (60–80 nm) (Figure 1b,e). The resulting particles carried a negative surface charge that decreased in absolute value with increasing ligand content on the particle surface (Figure 1c,f) due to decreasing numbers of carboxylic acid-terminated NMPs. Creating NPs with negative surface charges is a great method of avoiding nonspecific attachment to the negative cell membrane. To evaluate the effect of ligand density on the particle–cell interaction, NPs with low (20%), medium (40%), and high (80%) ligand densities were prepared. Since polymer-ligand coupling occurred prior to particle preparation, the predicted ligand density correlated well with the actual ligand density measured after particle preparation (Figure 1d,g).

2.2. AT1R-Binding of Ang-II Carrying NPs

To determine the effect that ligand mobility exerts on the AT1R interaction and the NP's overall avidity, $NP_{2/510}$ and $NP_{5/510}$ functionalized with Ang-II ($NP_{2/510}$Ang-II and $NP_{5/510}$Ang-II, respectively) carrying 20%, 40%, or 80% ligand densities were prepared. The affinities of the particle-bound ligands and avidities of the resulting formulations toward the AT1R after a short NP–cell contact were evaluated using a calcium mobilization assay (**Figure 2**) with AT1R-expressing rat mesangial cells (rMCs),[22] as previously described by our group.[22,28] Under normal conditions, rMCs express high levels of the AT1R, of about 1185 ± 83 fmol mg^{-1} protein.[29] The stimulation of the Gq-coupled AT1R by an agonist results in a cytosolic Ca^{+2} influx that is measured by this assay.[25] It is known that the binding of ligands to polymers like PEG reduces their affinity toward their target receptor[2] (Figure S3a, Supporting Information). Interestingly, the coupling of Ang-II to COOH–PEG_{5k}–PLA_{10k} resulted in even higher affinity loss than that measured for the PEGylated form. However, this is compensated through an avidity gain of NPs prepared from the aforementioned polymer (Figure S3b, Supporting Information), as they enable multivalent binding of the ligands to the cell membrane-bound receptors. The avidity of the particles (determined through the EC50 values obtained based on particle concentration (PNC-EC50)), was in the same nanomolar range for both particle types (Figure 2). However, there were notable differences between the two formulations regarding the effect of ligand density. While the avidity of $NP_{2/510}$ significantly increased with higher functionalization (Figure 2a), it remained constant for $NP_{5/510}$ (Figure 2b), even though the number of ligands per NP increased with the ligand density in both particle types (Figure S4, Supporting Information). This suggests that the rigid composition due to long NMPs of $NP_{5/510}$ hinders subsequent ligand–receptor interactions with increasing numbers of available ligands. This is reinforced by the fact that the overall affinity of the particle-bound ligands (LC-EC50) remained equal independent of the NP composition (Figure 2c,d). As the only parameter affecting multivalency varied between the formulations is the ligand mobility, the differences in avidity of $NP_{2/510}$ is most likely a result of the shorter NMPs.

However, in these experiments the NP–cell contact is very brief (under 1 min). As NPs are much larger than free ligands, they experience diminished diffusion, and thus require an extended presentation time to effectively interact with their targets. To investigate NP–cell interactions over a longer timescale, specifically how the avidity of $NP_{2/510}$Ang-II for the AT1R is affected, we extended the incubation period of the NPs with cells to 30 min (**Figure 3**) and determined the NP avidity (PNC-IC50) (Figure 3a) and the particle-bound ligand affinity (LC-IC50) (Figure 3b). After extensive NP–cell contact, the avidity of $NP_{2/510}$Ang-II increased (Figure 3a). However, this increase was only significant for particles with low (20%) ligand densities, i.e., highest ligand mobilities (Figure 3a). The particle-bound ligands also displayed increased affinities (IC50) for the AT1R compared to the ones obtained after a short stimulation (EC50) (Figure 3b) and the highest increase was also seen for $NP_{2/510}$ at low ligand densities (20%) (Figure 3b). These results indicate that a higher ligand mobility leads to a slower NP–cell interaction which can be explained by a lower number of ligands on the particle corona,[6] which necessitate extra time to execute binding. Additionally, reversible entrapment of the ligands in the polymer chains may occur,[30] impairing rapid

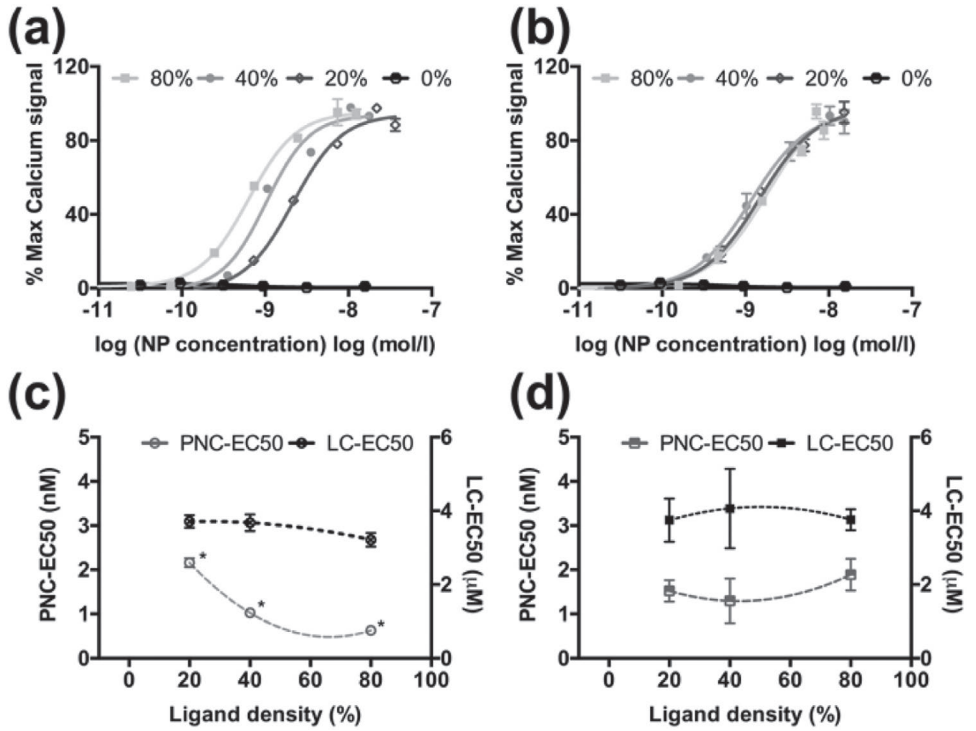

Figure 2. AT1R stimulation by Ang-II decorated NPs in rMCs. Maximum intracellular calcium response of $NP_{2/510}$Ang-II a) and $NP_{5/510}$Ang-II b) with different ligand densities. Particle avidity and ligand affinity of $NP_{2/510}$Ang-II c) and $NP_{5/510}$Ang-II d). PNC-EC50 (EC50 values calculated based on NP concentration); LC-EC50 (EC50 values calculated based on particle-bound ligand concentration). Results are presented as mean ± SD of at least $n = 3$ measurements. The data in (c) are fitted with a second-order polynomial. Levels of statistical significance are indicated as $*p \leq 0.001$ comparing PNC-EC50 values at different ligand densities.

ligand–receptor interactions. This phenomenon is more probable in NPs with low grafting densities[31] and long polymer chains.[32] The slower interactions of flexible particles may show potential benefits in vivo where NPs face extensive circulation times and, more importantly, off-target cells. As the selectivity of a multivalent system can be increased if initial binding is impeded by a repulsive factor,[9] the delayed initial binding of particles with high ligand mobility ($NP_{2/510}$ 20% ligand) (Figures 2 and 3) may be an alternative to the suggested approach of adding sterically hindering polymer chains.[33] Additionally, the inclusion of extra polymers, which can hinder the subsequent targeting efficiency, would be circumvented by this design. However, this needs to be further investigated in future experiments.

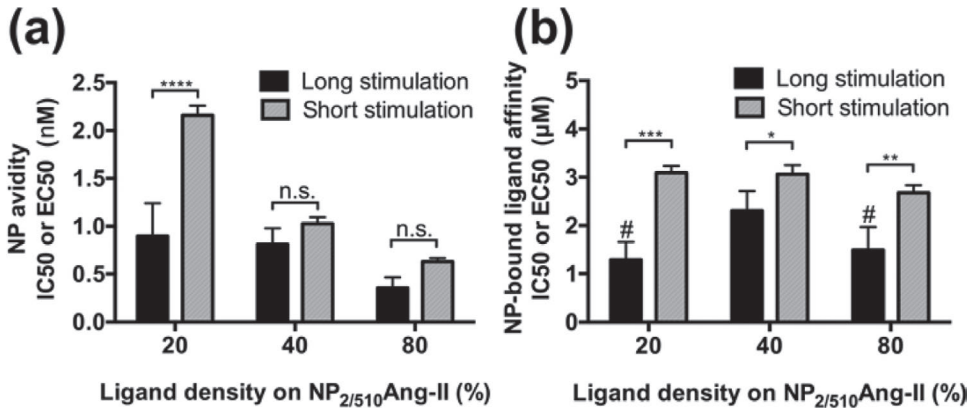

Figure 3. Influence of the AT1R stimulation period on the particle avidity a) and particle-bound ligand affinity b) of $NP_{2/510}$Ang-II. A short (1 min) direct stimulation of rMCs with the particles yields a dose response curve where the EC50 values can be calculated. By preincubating the cells with the NPs (30 min) and treating them afterward with free Ang-II, the IC50 values can be determined. Results are presented as mean ± SD of at least $n = 3$ measurements. Levels of statistical significance are indicated as $*p \leq 0.05$, $**p \leq 0.01$, $***p \leq 0.001$, and $****p \leq 0.0001$, and $\#p \leq 0.05$ compared to particle-bound ligand affinity at 40% ligand density n.s: nonsignificant.

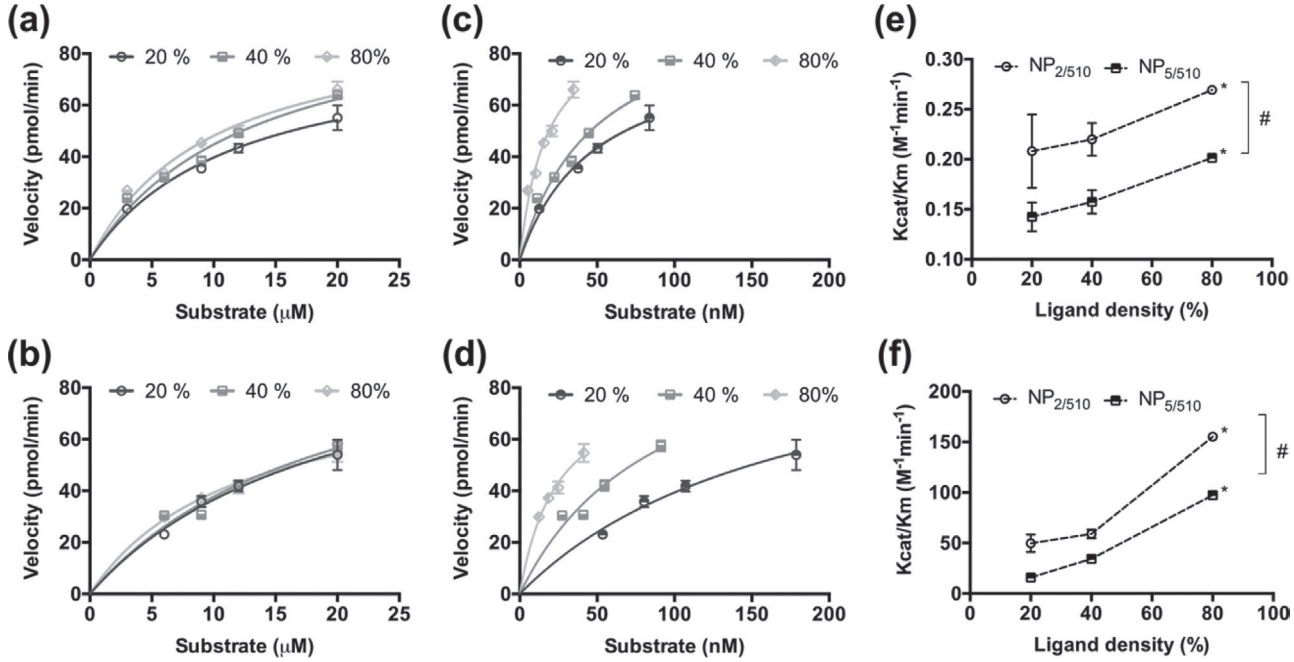

Figure 4. Michaelis–Menten kinetics of Ang-I decorated NPs. Enzyme kinetics calculated based on ligand concentrations of $NP_{2/510}$Ang-I a) and $NP_{5/510}$Ang-I b), or NP concentrations of $NP_{2/510}$Ang-I c) and $NP_{5/510}$Ang-I d) at different ligand densities. Specificity constant (Kcat/Km) of $NP_{2/510}$ and $NP_{5/510}$ calculated with the e) ligand- or f) NP concentration-based Km. Results are presented as mean ± SD of at least $n = 3$ measurements. Levels of statistical significance are indicated as $*p \leq 0.05$ comparing NPs with 80% ligand density to NPs with 20% or 40% ligand density and $\#p \leq 0.005$ comparing $NP_{2/510}$ and $NP_{5/510}$.

2.3. ACE Kinetics Using Ang-I Decorated NPs as Substrates

To explore the effect of ligand availability on the multivalent binding abilities toward an alternative target, we selected Ang-I-decorated NPs that interact with the cell membrane-bound ACE.[22] NPs with 20%, 40%, or 80% Ang-I modified PEG_{5k}–PLA_{10k} were prepared, with particle coronas made up of either short COOH–PEG_{2k}–PLA_{10k} or long COOH–PEG_{5k}–PLA_{10k} NMPs ($NP_{2/510}$Ang-I and $NP_{5/510}$Ang-I, respectively). Soluble ACE obtained from rabbit lung served as a surrogate for the cell membrane-bound form of the enzyme to determine the Michaelis–Menten kinetics for the different particles (**Figure 4**). The Michaelis–Menten constant (Km) was calculated based on the ligand (Figure 4a,b) and particle concentrations (Figure 4c,d) for the different NP formulations (Table S1, Supporting Information). Additionally, the catalysis constant (Kcat) was determined to calculate the specificity constant (Kcat/Km), which is useful in comparing different substrates for the same enzyme[34] (Figure 4e,f). The substrate that yields the highest specificity constant is considered the best substrate for the enzyme. At all ligand densities, the Kcat/Km values for $NP_{2/510}$ were significantly higher than those for $NP_{5/510}$, for both ligand- (Figure 4e) and NP concentration-based (Figure 4f) calculations. This suggests that the ligands on their surface are better accessible to the enzyme, which can be attributed to the shorter NMPs. For both $NP_{2/510}$ and $NP_{5/510}$, the affinity for the enzyme increases with higher ligand density, probably due to a higher number of ligand molecules on the NP surface (Figure S4, Supporting Information) that are able to bind more enzyme molecules. Nevertheless, because a soluble form of ACE was used for the experiments, the ligand-enzyme interaction is not spatially constrained as it would be with the cell membrane-bound enzyme and cannot fully illustrate the multivalent binding on a cellular surface.

2.4. Cellular Internalization of AT1R-Targeting NPs

To determine the influence of ligand mobility at a cellular level we performed uptake experiments (**Figure 5**) analyzed via flow cytometry (Figure 5a) and confocal laser scanning microscopy (CLSM) (Figure 5b). rMCs, positive for AT1R expression, were used as target cells.[22] Considerable differences could be detected between Ang-II decorated $NP_{2/510}$ and $NP_{5/510}$. In agreement with our previous experiments, uptake was noticeably dependent on ligand density for $NP_{2/510}$. However, lower ligand densities (20%) resulted in much better cellular internalization than medium- (40%) or high (80%) ligand densities, differing from what would be expected by the AT1R-avidity measurements performed at short stimulation periods (Figure 2). These divergencies can be explained by the fact that for NP uptake the cells are incubated for longer time periods (45 min) with the NPs. As can be seen for the avidity measurements after a long stimulation (Figure 3), the avidity of the particles evens out at all ligand densities. Additionally, it can be attributed to differences in experimental setup, as uptake experiments are performed with adherent cells, mimicking physiological conditions, and for the avidity measurements cells must be placed in suspension. Under such nonrestrictive conformational conditions,

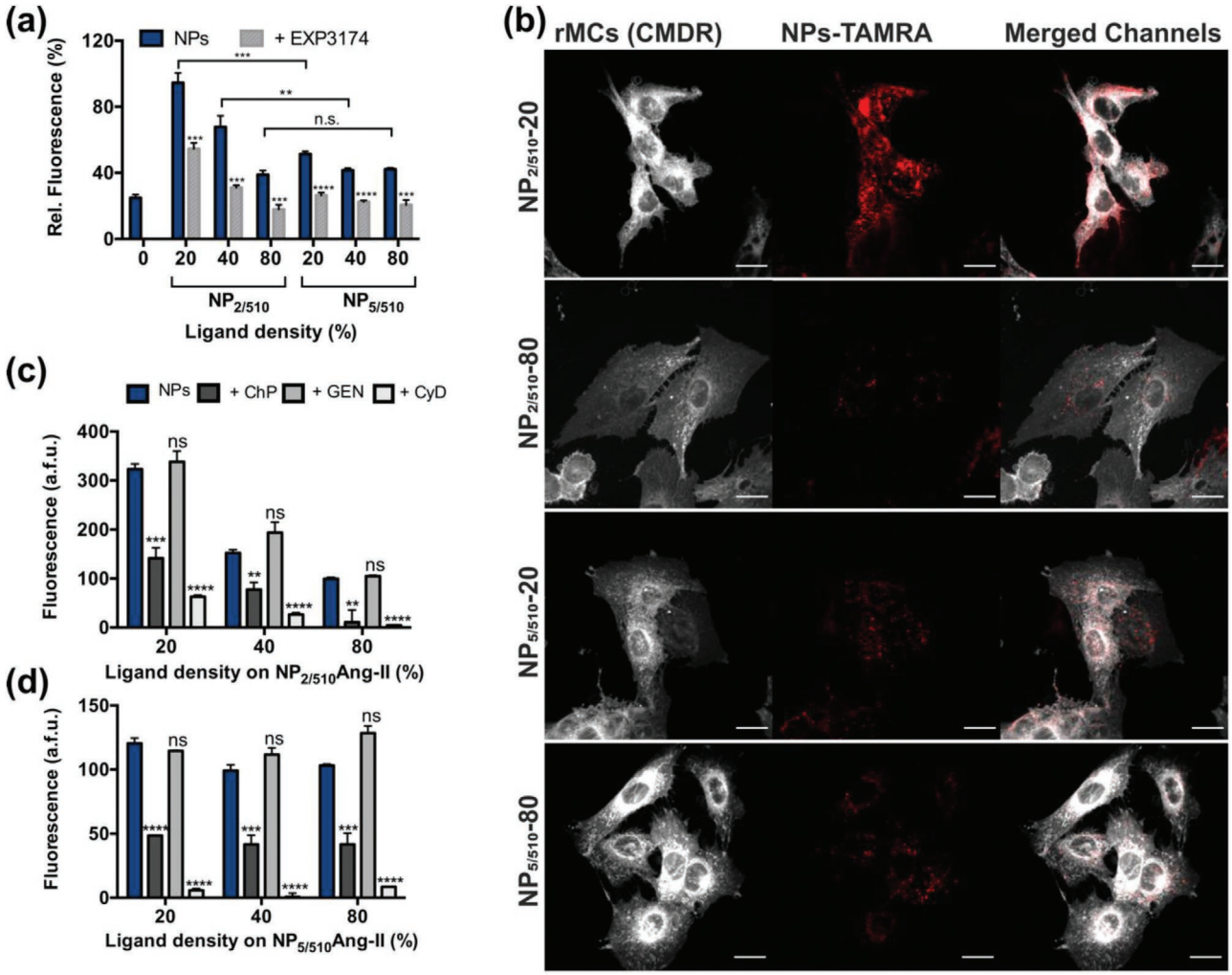

Figure 5. Cellular internalization of $NP_{2/510}$Ang-II and $NP_{5/510}$Ang-II in rMCs. Uptake of NPs with different ligand densities and uptake inhibition by free EXP3174 analyzed by flow cytometry a). Uptake of $NP_{2/510}$Ang-II and $NP_{5/510}$Ang-II with 20% or 80% ligand density analyzed by CLSM (Scale bar 20 μm) b). Internalization inhibition of $NP_{2/510}$Ang-II c) and $NP_{5/510}$Ang-II d) by chlorpromazine (ChP), genistein (GEN), or cytochalasin D (CyD). Results are presented as mean ± SD of at least $n = 3$ measurements. Levels of statistical significance are indicated as $^{**}p \leq 0.005$, $^{***}p \leq 0.0005$, and $^{****}p \leq 0.0001$. n.s.: nonsignificant.

receptor interactions at higher ligand densities may be favored.

$NP_{5/510}$-associated fluorescence was independent of the degree of functionalization, mirroring the AT1R avidity measured by the intracellular calcium assay described above. This indicates that a lower ligand mobility constrains the ligand–receptor interaction. When rMCs were incubated with an AT1R antagonist, losartan carboxylic acid (EXP3174), for 30 min, we observed significant suppression of uptake which suggests specificity. Overall, $NP_{2/510}$ were taken up to a much higher extent than $NP_{5/510}$, demonstrating that shorter 2k NMPs that enhance the ligand mobility facilitate the NP–cell interaction. It points toward a better receptor binding, as higher internalization rates are usually related to enhanced multivalent binding.[35] With 80% ligand density, the uptake of $NP_{2/510}$ matches that of $NP_{5/510}$, as the particles assimilate, and the ligands lose mobility due to an increase in long LMPs. At 80% ligand density, 80% of the PEG on the particle surface is long 5k PEG, and only the remaining 20% is the shorter 2k for $NP_{2/510}$ or longer 5k PEG for $NP_{5/510}$. With this polymer composition, it seems that the favorable effects of shorter NMPs are lost, as there are majority of longer polymer chains hindering the ligand binding. These results highlight the importance of ligand mobility to obtain satisfactory cellular interaction. Contrary to common assumptions that increasing the degree of functionalization increases the targeting potential of NPs, here we demonstrate that the amount of ligand present on the surface is not as important as its mobility, i.e., the conformational flexibility that allows it to interact with the target receptors. Similar effects were described by Poon et al. for folate-functionalized particles. They noticed that increasing the surface coverage over the optimal 20% lead to less efficient NP uptake.[36] Furthermore, an increase in ligand density usually reduces the targeting potential due to enhanced serum protein adsorption resulting from covering the PEG shield with ligands. Minimizing protein corona formation is essential to preserve the specific targeting abilities of

nanomaterials[37] and avoid their clearance by macrophages.[38] For our formulations, significantly higher serum protein adsorption was observed for rigid $NP_{5/510}$ compared to flexible $NP_{2/510}$ (Figure S5, Supporting Information). This seems to corroborate our assumption that LMPs on flexible particles can assume a partially folded conformation, which initially may shield the ligand. This trend is enhanced with lower particle functionalization.

Intracellular localization of the NPs was confirmed by CLSM analysis (Figure 5b). For microscopy experiments, only particles with low (20%) and high (80%) ligand densities were investigated. NPs with medium (40%) ligand density were not examined because minor differences between particle types are difficult to discern by this method. The results mirrored those obtained by flow cytometry. The highest NP-associated fluorescence was seen for $NP_{2/510}$ with 20% ligand on the surface. At 80% ligand density, uptake of $NP_{2/510}$ is comparable to that of $NP_{5/510}$, which shows no dependency with the ligand density. The uptake could be inhibited by EXP3174 treatment of cells prior to NP addition (Figure S6, Supporting Information).

To investigate if ligand mobility influences the internalization pathway of Ang-II functionalized NPs, we performed uptake inhibition studies by preincubating the cells with either chlorpromazine, genistein, or cytochalasin D (clathrin, caveole, or actin polymerization inhibitors, respectively) prior to NP addition. As shown in Figure 5c,d, adding chlorpromazine significantly inhibited uptake of Ang-II carrying NPs by about 60–80%. This level of inhibition was similar to that caused by EXP3174, indicating that particles are mainly taken up by specific clathrin-mediated endocytosis. We previously found the same uptake pathway for Ang-II decorated quantum dots.[28] Genistein did not affect NP uptake, indicating that it is not caveolae-mediated. As expected, Cytochalasin D caused the highest uptake inhibition, as it is able to inhibit both nonspecific particle uptake as well as interfere with other endocytic routes like clathrin-mediated endocytosis by disrupting the cell cytoskeleton.[39,40] Regarding the internalization route, no differences could be detected between the different formulations, indicating that increased ligand mobility just enhances the multivalent binding of the receptor, without changing the natural endocytic route.

2.5. Cellular Internalization of Ang-I Decorated NPs

To determine the influence of ligand mobility on the uptake of enzyme targeting particles, we also determined the cellular uptake of ACE-targeting Ang-I decorated NPs ($NP_{2/510}$Ang-I and $NP_{5/510}$Ang-I) (**Figure 6**), via flow cytometry (Figure 6a) and CLSM (Figure 6b) in rMCs.[22] Ang-I is a substrate for ACE and when it is located on the particle corona it binds to the enzyme on the cell membrane. This results in the production of Ang-II on the particle surface and the NPs can then be internalized by AT1R-mediated endocytosis.[22] Interestingly, the uptake results for Ang-I decorated NPs mirrored the results for Ang-II decorated NPs. Higher uptake was obtained for $NP_{2/510}$ compared to $NP_{5/510}$, which decreased with increasing ligand density. The specificity of uptake via the AT1R was proven by the significant suppression observed after addition of captopril, an ACE inhibitor (Figure 6a). The similarity between the uptake of Ang-I and Ang-II decorated NPs indicates that the initial conversion of Ang-I on the particle surface is not a limiting factor for particle internalization. Furthermore, when comparing the uptake kinetics of Ang-I and Ang-II decorated NPs, equivalent results were obtained (Figure 6c,d). Because the enzymatic conversion of Ang-I to Ang-II occurs rapidly on the rMC surface (2 pmol min^{-1}),[22] it does not limit cellular uptake as much as multivalent AT1R binding. Under these experimental conditions, the Ang-I on the particle surface is converted to Ang-II in less than 1 min by the cells. With a 45 min incubation period, this leaves the particles enough time to interact with the AT1R. Additionally, the higher uptake of Ang-I modified $NP_{2/510}$ is favored by the higher affinity of the ligands to the enzyme (Figure 4), which keeps them at the cell surface facilitating subsequent receptor binding. Equivalent results were obtained by CLSM analysis (Figure 6b; and Figure S7, Supporting Information), which confirmed intracellular localization of NPs.

2.6. Polymer Distribution on the NP Shell: Conformational Considerations and Distance between PEG Chains

To explain the differences between the NP formulations regarding interaction with their targets, we estimated the distance between the PEG chains on the particle corona. The theoretical distance between the polymer chains on a particle corona for a known NP diameter and polymer molecular weight can be calculated assuming that all the PEG from the PEG-PLA blockcopolymer migrates to the outer NP shell and the PLA blocks are anchored in the core[12] (see the Experimental Section for an exact explanation of the calculation). In this way we determined the distance between NMPs (*ds*), LMPs (*D*), and LMPs and the next same-length polymer (*Ds*) (**Figure 7**; and Table S2, Supporting Information). The *ds* values for $NP_{2/510}$ and $NP_{5/510}$ are comparable, as the total polymer in both formulations is the same and increases with the ligand density (Figure 7b). *D* also follows the same trend for the two NP formulations, with decreasing distances at higher LMP content (Figure 7c). Nevertheless, when *Ds* is calculated, significant differences between the two NP species are detected (Figure 7d). For $NP_{5/510}$, *Ds* remains constant, independent of the amount of ligand that the particles carry, because all the polymer chains are exactly the same length. For $NP_{2/510}$, there is a significant decrease in *Ds* as more, longer LMP chains are added to the formulation. Furthermore, there is a significantly higher *Ds* for all ligand densities compared to $NP_{5/510}$, due to the shorter NMPs. This indicates that the ligands have higher mobility freedom and are less sterically hindered on $NP_{2/510}$ than on $NP_{5/510}$. As the particles assimilate to $NP_{5/510}$ at higher ligand densities this distance diminishes, and the particles become more rigid. Depending on the size of the target receptor or enzyme, the distance between ligands can highly influence the outcome of an interaction, as not all ligands may be able to bind. According to Erickson, the approximate radius of a protein in nm can be calculated assuming a spherical shape and an average specific volume of 0.73 cm^3 g^{-1}.[41] The AT1R is a protein composed of 359 amino acids with a molecular weight of ≈41 kDa.[42] The ACE has a molecular weight of 112 kDa.[43] Under the

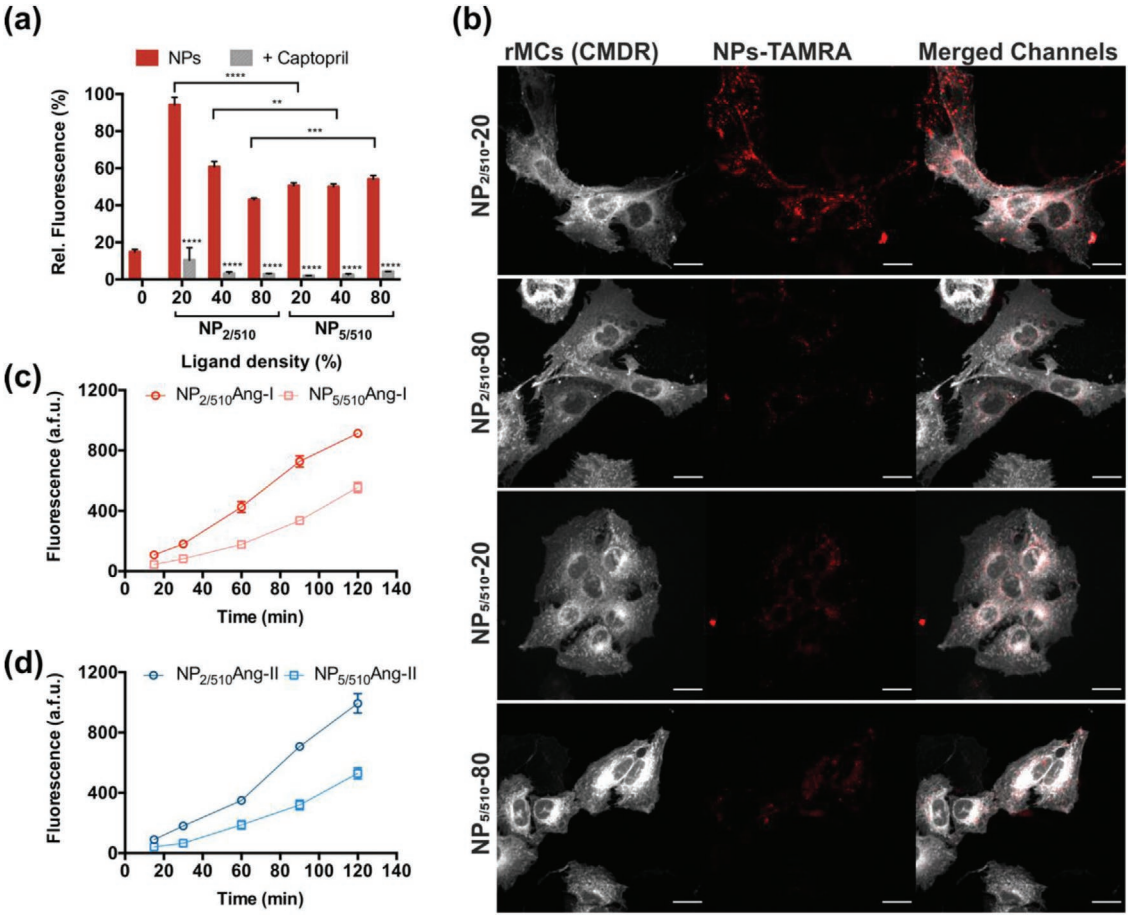

Figure 6. Cellular internalization of $NP_{2/510}$Ang-I and $NP_{5/510}$Ang-I in rMCs. Cellular uptake of NPs with different ligand densities and internalization inhibition by 1×10^{-3} M captopril analyzed by flow cytometry a). Uptake of $NP_{2/510}$Ang-I and $NP_{5/510}$Ang-I with 20% or 80% ligand density analyzed by CLSM (Scale bar 20 µm) b). Internalization kinetics of Ang-I c) or Ang-II d) functionalized $NP_{2/510}$ and $NP_{5/510}$ with 20% ligand density. Results are presented as mean ± SD of at least $n = 3$ measurements. Levels of statistical significance are indicated as $^{**}p \leq 0.005$, $^{***}p \leq 0.0005$, and $^{****}p \leq 0.0001$.

aforementioned assumptions, the diameters of the AT1R and ACE would be ≈4.6 and 6.4 nm, respectively. According to this, only the flexible particles ($NP_{2/510}$) with low ligand density would be able to bind several targets in a multivalent manner (Figure 7d). At higher degrees of functionalization, the distance between consecutive ligands is smaller than the one between targets, leading to inefficient binding where some ligands may lose their targeting capacity and sterically hinder each other. For rigid NPs ($NP_{5/510}$), the long NMPs can also limit the LMP mobility and prevent the ligands from interacting with their targets. This explains the superior NP–cell interaction displayed by $NP_{2/510}$ (Figures 5 and 6), where the ligands have a higher conformational freedom to bind their targets, a trait conferred by the shorter NMPs. To further confirm the arrangement of the PEG chains on the particle surface, the Flory radius (R_F) was calculated. If the distance between polymer chains is greater than R_F, the polymers assume a folded mushroom configuration. When R_F is greater than the distance between polymer chains, they adopt an extended brush conformation.[30] The R_F values calculated for the 2k and 5k PEGs were 3.60 and 6.06 nm. For all NP formulations, the distances between the PEG chains on the particle surface were less than the R_F (Figure S8, Supporting Information), suggesting a brush conformation. For the low ligand density $NP_{2/510}$ the distance between LMPs is over the R_F value of 2k PEG but under that for 5k PEG. Taken all together, this can explain the higher mobility and flexibility of the LMPs at lower ligand densities in $NP_{2/510}$, for which there could be a partially folded configuration that would make interactions of such particles slower but more efficient regarding binding and its subsequent cellular uptake.

3. Conclusion

The establishment of multivalent interactions between NPs and their target cells is a complex multifactorial process. Different particle attributes, such as size or ligand- type and density[5] are essential for determining the binding avidity. However, our work suggests that a high particle avidity for the targeted receptors does not unequivocally predict a particle's fate after binding.

In this study, we demonstrated that by tailoring the polymer composition on the particle corona, the ligand mobility, and in turn the cellular uptake of NPs can be modulated. By combining

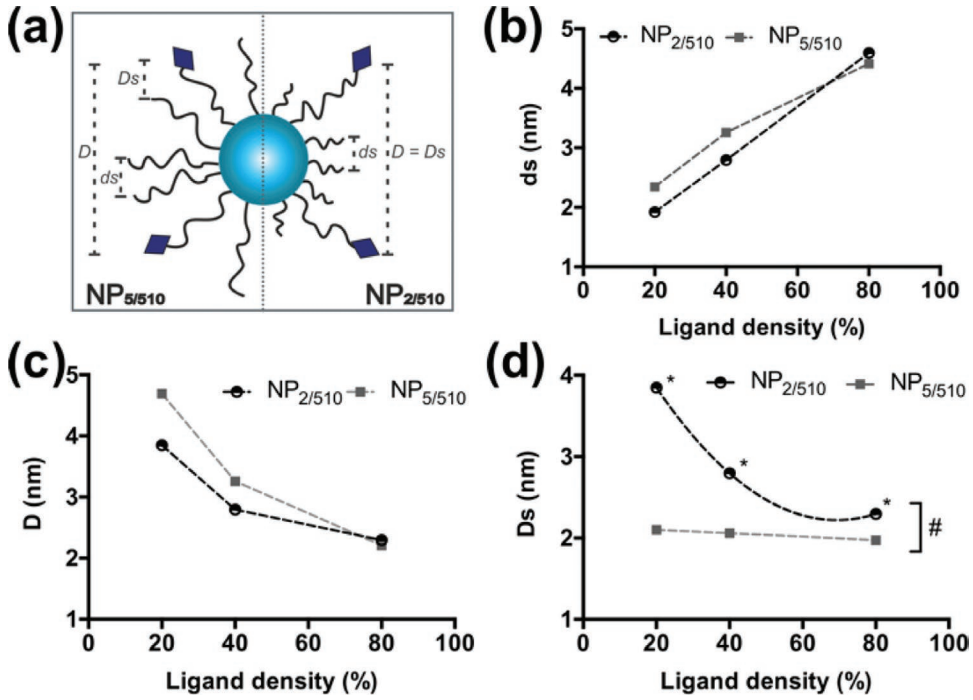

Figure 7. Distance between polymer chains on the NP corona at different ligand densities. Schematic representation of the distance among polymer chains on $NP_{2/510}$ and $NP_{5/510}$ a). Distance *ds* between NMPs b), distance *D* between ligand-modified polymer chains c) and distance *Ds* between ligand-modified polymer and the same length PEG chains d). Results are presented as mean ± SD of at least $n = 3$ calculations derived from at least $n = 3$ independent size measurements. The data in (d) were fitted with a second-order polynomial. Levels of statistical significance are indicated as $*p \leq 0.0001$ comparing $NP_{2/510}$ with 20%, 40%, and 80% ligand densities and $\#p \leq 0.0001$ comparing $NP_{2/510}$ and $NP_{5/510}$ at different ligand densities.

polymers of different lengths, we were able to design particles with high polymer density, which is essential for stealth properties,[44] while still preserving the mobility of the tethered ligands. We showed that flexible particles ($NP_{2/510}$) with the highest ligand mobility (at 20% ligand density) even though partially subjected to ligand shrouding have analogous avidities for their targets to their rigid counterparts ($NP_{5/510}$) which present more surface-available but sterically hindered ligands. More so, after extensive cellular contact the interactions with the targets are facilitated and thus, the particles' avidities and particle-bound ligand affinities significantly increased. Furthermore, flexible particles experience increased cellular uptake due to the optimal distance between targeting entities along with a higher ligand mobility. Interestingly, increasing the ligand density did not result in higher targeting ability of the NPs, due to a sterically hindered, inefficient target binding. Thus, it is advisable to avoid overloading NPs with ligands, which can potentially lead to less selective binding,[8,9] and instead adjust the ligand mobility. The initial ligand shrouding should be further investigated, as it may have the potential to reduce initial binding, a strategy suggested to increase particle selectivity.[9,33] In this regard, the relationship of the formulation's avidity and binding with the receptor density would need to be elucidated. It is reasonable to believe that higher receptor densities may lead to increased cellular interactions. A phenomenon heightened the more flexible the formulations is, as the number of possible bindings increases.[8]

Taken together, our results show that designing of multivalently-binding NPs is an intricate process which necessitates finding a balance between several particle attributes. Among them, we show that the ligand mobility, which can be increased by adjusting the polymer corona composition and the number of targeting entities on the particle surface, needs to be considered to achieve optimal interactions at the cellular level.

4. Experimental Section

Materials: Carboxylic acid end-functionalized hydroxyl-PEG with molecular weights of 2000 (COOH–PEG_{2k}–OH) and 5000 Da (COOH–PEG_{5k}–OH) were obtained from JenKem Technology USA Inc. (Allen, TX). Lysine N-modified Angiotensin-I (Lys-Ang-I) and Ang-II (Lys-Ang-II) (purity > 98%) were purchased from Genscript (Piscataway, NJ). EXP3174 was purchased from Santa Cruz Biotechnology (Dallas, TX). Fura-2AM was purchased from Life Technologies (Carlsbad, CA). CellMask deep red plasma membrane stain (CMDR), and Pierce bicinchoninic acid (BCA) assay kit were purchased from Thermo Fisher Scientific (Waltham, MA). ACE from rabbit lung and all other reagents in analytical grade were obtained from Sigma-Aldrich (Taufkirchen, Germany). Ultrapure water was obtained from a Milli-Q water purification system (Millipore, Billerica, MA).

Cell Culture: rMCs were kindly gifted by Prof. Armin Kurtz (Institute of Physiology, University of Regensburg, Germany). They were cultured in RPMI1640 medium with 10% fetal bovine serum (Biowest, Nuaillé, France) supplemented with insulin-transferrin-selenium (Life Technologies, Carlsbad, CA) and 100×10^{-9} M hydrocortisone. The characterization of the cells for their AT1R and ACE expression was previously shown by the group.[22]

Polymer Synthesis and Ligand Coupling: PEG–PLA block-copolymers were synthesized via ring opening polymerization of cyclic lactide after Qian et al.[45] with slight modifications described previously by

the group.[46] COOH–PEG–OH was used as a macroinitiator and 1,8-diazabicyclo[5.4.0]undec-7-ene (DBU) as a catalyst. Resulting polymers were 10 kDa PLA with either a 2 or 5 kDa carboxylic acid terminated PEG chain (COOH–PEG_{2k}–PLA_{10k} or COOH–PEG_{5k}–PLA_{10k}, respectively).[22]

To synthesize Ang-I/II-PEG_{5k}–PLA_{10k}, COOH–PEG_{5k}–PLA_{10k} (14 µmol) was activated with 1-Ethyl-3-(3-dimethylaminopropyl)carbodiimide and N-Hydroxysuccinimide (350 µmol) in N,N-Dimethylformamide (DMF) for 2 h under stirring. Afterward, 2-Mercaptoethanol (863 µmol) was added to quench the reaction for 20 min. Either Lys-Ang-I or Lys-Ang-II ligand (17 µmol) were dissolved in DMF with N,N-Diisopropylethylamine (66 µmol), added dropwise to the activated polymer, and left to stir for 48 h. The resulting polymer was diluted in Millipore water so that the DMF content was lower than 10% v/v and dialyzed using a 6–8 kDa molecular weight cut-off regenerated cellulose dialysis membrane (Spectrum Laboratories, Inc, Rancho Dominguez, CA) for 24 h (with medium change after 30 min, 2, and 6 h) to remove uncoupled ligand and reagents. To determine the degree of ligand modification, polymer micelles were created by precipitating ACN-dissolved polymer in Millipore water under stirring to a final concentration of 1 mg mL^{-1}. After the complete evaporation of the organic phase, a Pierce BCA assay, following the manufacturer's instructions, and an iodine complexing colorimetric assay,[47] as previously described,[16] were performed to quantify the ligand and PEG concentration, respectively (Figure S1, Supporting Information).

NP Preparation: For preparation of block copolymer NPs, 10 mg mL^{-1} of either COOH–PEG_{2k}–PLA_{10k} or COOH–PEG_{5k}–PLA_{10k} (for $NP_{2/510}$ or $NP_{5/510}$, respectively) and $PLGA_{13.4k}$ were mixed in ACN at a 70:30 mass ratio. NPs were prepared via bulk nanoprecipitation under vigorous stirring in 10% Dulbecco's phosphate buffered saline (DPBS) v/v (pH 7.4) to a final concentration of 1 mg mL^{-1}. The NPs were left stirring for 3 h until the organic solvent was completely evaporated. Afterward, they were concentrated using a 30 kDa molecular weight cut-off Microsep advance centrifugal device (Pall Corporation, Port Washington, NY) at 959 *g* for 20 min. For particles with different ligand densities, the unmodified carboxylic acid-ended polymers were replaced by varying amounts of Ang-I/II-PEG_{5k}–PLA_{10k}, keeping the molar ratio of PEG chains to PLGA constant. For fluorescently-labeled NPs, a CF647- (for flow cytometry analysis) or TAMRA- (for CLSM experiments) covalently labeled PLGA, synthesized as described before by the group,[16] was used for NP preparation.

NP Characterization: Size and ξ-potential of all NP formulations were measured using a Malvern ZetaSizer Nano ZS (Malvern Instruments GmbH, Lappersdorg, Germany) with a 633 nm He-Ne laser at a backscatter angle of 173°. Size was measured in disposable microcuvettes (Brand, Wertheim, Germany). Electrophoretic mobility was measured using a folded capillary cell (Malvern, Herrenberg, Germany) with a set measurement position at 4.65 mm. Data were recorded using the Malvern Zetasizer software 7.11 (Malvern Instruments, Worcestershire). All samples were measured at 25 °C in 10% v/v DPBS (pH 7.4). PEG concentration in NPs was quantified using a colorimetric iodine complexing assay[47] and correlated with the exact gravimetrical NP content determined through lyophilization, as previously described by the group.[16] The molar NP concentration was calculated using Equation (1), where *m* is the NP mass determined through the iodine assay, ρNP is the density of the NPs (1.25 g cm^{-3}),[48] *dh* is the hydrodynamic diameter of the NPs measured by DLS, N_A is the Avogadro number, and *V* is the volume of the NP samples

$$\mathrm{PNC} = \frac{m}{\rho\mathrm{NP}\,\frac{4}{3}\pi\left(\frac{dh}{2}\right)^3} \times \frac{1}{N_A\,V} \quad (1)$$

Ligand content on NPs was quantified using a BCA assay, using Lys-Ang-I and Lys-Ang-II as standards, following the manufacturer's instructions, and normalized to the molar PEG concentration to obtain the ligand density. Absorbance measurements were performed with a FLUOstar Omega microplate reader (BMG Labtech, Ortenber, Germany).

Intracellular Calcium Measurements: To quantify the AT1R response to the different NP formulations, a ratiometric Fura-2 Ca^{2+} chelator method[49] was used as previously described by the group.[2] In short, a rMC-suspension was incubated in Leibovitz medium (LM) supplemented with 5×10^{-6} M Fura-2AM, 0.05% Pluronic F-127, and 2.5×10^{-3} M Probenecid (1 h, light protected, 50 rpm). The cells were washed with DPBS by centrifugation (2x, 200 *g*, 5 min) and adjusted to a count of either 2 or 1 million cells mL^{-1} (for IC50 or EC50 measurements, respectively) in LM with 2.5×10^{-3} M Probenecid. To determine EC50 values (short stimulation) cells (90 000 cells) were injected on top of the samples (10 µL, 1×10^{-9} M to 300×10^{-6} M ligand concentration) and the resulting signal recorded immediately for 30 s per well using a FLUOstar Omega microplate reader. Filters used for excitation were 340/20 and 380/20 nm, and the emission was recorded with a 510/20 nm bandpass filter. To determine IC50 values (long stimulation), samples (10 µL,1×10^{-9} M to 300×10^{-6} M ligand concentration) were incubated with 90 000 cells in a half-area microplate plate for 30 min. Afterward, an Ang-II solution (45 µL, 300×10^{-9} M) was injected on top of the samples and the calcium influx was measured as described above. 0.1% Triton-X 100 or 0.1% Triton-X 100 with 45×10^{-3} M ethylene glycol-bis(2-aminoethylether)-N,N,N′,N′-tetraacetic acid were used as control solutions to determine the maximal and minimal signal ratio (Rmax and Rmin). The intracellular calcium concentrations were calculated with an assumed K_d value of 255×10^{-9} M for the fura-2-calcium complex, after Grynkiewicz.[49] The maximum calcium signal (%) was plotted against the molar NP concentration, calculated after Equation (1), to allow comparison between formulations. Statistical significance was assessed by a Student's *t* test using GraphPad Prism 6.0 (GraphPad Software Inc. La Jolla, CA).

Enzyme Kinetic Measurements: The Michaelis–Menten kinetics of the soluble form of ACE were determined using Ang-I bearing NP formulations as the substrate. To that end, the different NP formulations (ligand concentrations 10–200 $\times 10^{-6}$ M) were incubated with rabbit lung ACE (18×10^{-6} M) for different time periods (5, 15, 30, 60, 90, and 120 min). The conversion over time of Ang-I to Ang-II on the particle corona was quantified by measuring the intracellular calcium influx generated by the AT1R stimulation by the hydrolyzed substrate, as described above. A range of known concentrations of Ang-II (1×10^{-9} M–300×10^{-6} M) were used as control samples in the assay to convert the measured calcium concentration ($\times 10^{-9}$ M) to pmol of product. The velocity of the reaction (pmol min^{-1}) at 15 min incubation time was plotted against the substrate concentration used in the assay to determine the Michaelis–Menten constant (Km) using GraphPad Prism 6.0. The catalytic constant (Kcat) was determined and the specificity constant (Kcat/Km) used to compare different substrates for one enzyme. A Student's *t* test was performed with GraphPad Prism 6.0 to assess statistical significance.

Flow Cytometry: To determine the uptake rates of the different NP formulations via flow cytometry, rMCs were seeded in 24-well plates (30 000 cells per well) and incubated over 48 h. Afterward, they were incubated for 45 min with CF647-labeled NP solutions (20 µg mL^{-1}) in LM supplemented with 0.1% BSA. To inhibit the NP uptake, the cells were preincubated with either EXP3174 (1×10^{-3} M) or chlorpromazine, genistein, or cytochalasin D (25×10^{-6} M) in LM for 30 min prior to NP addition. Next, the cells were washed with DPBS, trypsinized and washed through centrifugation with DPBS (2x, 200 *g*, 5 min, 4 °C). Finally, the NP-associated cell fluorescence was analyzed using a CyFlow Space flow cytometer (Sysmex Partec GmbH, Goerlitz, Germany) with FloMax software. A 638 nm red diode laser was used to excite, and a 675/30 bandpass filter was used to record fluorescence. Data were analyzed using Flowing software (Turku Centre for Biotechnology, Finland). The population of viable cells was gated, and the fluorescence geometrical mean was evaluated. GraphPad Prism 6.0 was used to asses statistical significance through a Student's *t*-test.

CLSM Analysis: To analyze NP uptake using CLSM, rMCs were seeded into 8-well Nunc Lab Tech II Chamber Slide systems (Thermo Fisher Scientific, Waltham, MA) (10 000 cells per well) and left to attach for 24 h. After that, the cells were washed with DPBS and incubated with TAMRA-labeled NPs (20 µg mL^{-1}) in LM supplemented with 0.1% BSA for 45 min. After the incubation period, the NP solutions were discarded, and the cells were washed with DPBS and stained fluorescently with CMDR (1x) for 5 min before fixing them with 4% paraformaldehyde in DPBS (10 min, r.t.). To inhibit the NP uptake, the cells were pretreated with EXP3174 (1×10^{-3} M) in LM with 0.1% BSA for 30 min prior to NP addition. Images were acquired with AIM4.2 software (Zeiss, Jena, Germany) using a Zeiss Axiovert 200 microscope with an LSM 510 laser-scanning device using a 63x Plan-Apochromat (NA 1.4) objective. Fluorescence was excited with 543 and 633 nm He-Ne lasers and recorded with a 560–615 bandpass and a 650 longpass filter (for NP and cell fluorescence, respectively). The focal plane was set at 1.5 µm.

Calculation of the Distance between PEG Chains (D, Ds, and ds): The surface (*S*) that each PEG chain occupies on the NP was calculated after Gref et al.[12] using Equation (2) where M_{PEG} is the molecular weight of the PEG chains and f is the mass fraction of PEG in the blends of PEG-PLA. Subsequently the distance between PEG chains was determined through Equation (3), assuming that *S* is a circular area,[50] and a homogeneous polymer distribution. The parameters used for the calculations are listed in Table S2 (Supporting Information). The R_F was calculated as an indicator of the arrangement of the PEG chains on the NP surface with Equation (4) where the length of a PEG monomer is $\alpha = 0.35$ nm and the number of monomers in one molecule (N) was determined by dividing the molecular weight of the PEG by the monomer molecular weight of 44 g mol^{-1}

$$S = \frac{6\,M_{PEG}}{dh\,N_A\,f\,\rho NP} \tag{2}$$

$$D = 2\left(\frac{S}{\pi}\right)^{\frac{1}{2}} \tag{3}$$

$$R_F = \alpha N^{\frac{3}{5}} \tag{4}$$

Supporting Information

Supporting Information is available from the Wiley Online Library or from the author.

Acknowledgements

The authors thank Renate Liebl and Viktoria Eismann for their excellent technical assistance. Financial support from the German Research Foundation (DFG), Grant No. GO 565/17-3, is gratefully acknowledged.

Conflict of Interest

The authors declare no conflict of interest.

Keywords

cellular interactions, ligand density, ligand mobility, multivalency, polymer nanoparticles

Received: December 16, 2019
Revised: January 27, 2020
Published online: February 20, 2020

[1] T. M. Allen, P. R. Cullis, *Science* **2004**, *303*, 1818.
[2] R. Hennig, K. Pollinger, A. Veser, M. Breunig, A. Goepferich, *J. Controlled Release* **2014**, *194*, 20.
[3] S. Hong, P. R. Leroueil, I. J. Majoros, B. G. Orr, J. R. Baker, M. M. Banaszak Holl, *Chem. Biol.* **2007**, *14*, 107.
[4] D. R. Elias, A. Poloukhtine, V. Popik, A. Tsourkas, *Nanomedicine* **2013**, *9*, 194.
[5] A. M. Alkilany, L. Zhu, H. Weller, A. Mews, W. J. Parak, M. Barz, N. Feliu, *Adv. Drug Delivery Rev.* **2019**, *143*, 22.
[6] H. Yuan, S. Zhang, *Appl. Phys. Lett.* **2010**, *96*, 033704.
[7] C. Dalal, A. Saha, N. R. Jana, *J. Phys. Chem. C* **2016**, *120*, 6778.
[8] K. C. Tjandra, P. Thordarson, *Bioconjugate Chem.* **2019**, *30*, 503.
[9] T. Curk, J. Dobnikar, D. Frenkel, *Multivalency Concepts, Research & Applications*, Wiley, Hoboken, NJ **2018**, pp. 75–102.
[10] P. I. Kitov, D. R. Bundle, *J. Am. Chem. Soc.* **2003**, *125*, 16271.
[11] A. L. Klibanov, K. Maruyama, V. P. Torchilin, L. Huang, *FEBS Lett.* **1990**, *268*, 235.
[12] R. Gref, M. Lück, P. Quellec, M. Marchand, E. Dellacherie, S. Harnisch, T. Blunk, R. Müller, *Colloids Surf., B* **2000**, *18*, 301.
[13] D. E. Owens Iii, N. A. Peppas, *Int. J. Pharm.* **2006**, *307*, 93.
[14] L. J. Cruz, P. J. Tacken, R. Fokkink, C. G. Figdor, *Biomaterials* **2011**, *32*, 6791.
[15] J. F. Stefanick, J. D. Ashley, T. Kiziltepe, B. Bilgicer, *ACS Nano* **2013**, *7*, 2935.
[16] K. Abstiens, M. Gregoritza, A. M. Goepferich, *ACS Appl. Mater. Interfaces* **2019**, *11*, 1311.
[17] W. Jiang, B. Y. S. Kim, J. T. Rutka, W. C. W. Chan, *Nat. Nanotechnol.* **2008**, *3*, 145.
[18] Y. Liu, K. Li, J. Pan, B. Liu, S.-S. Feng, *Biomaterials* **2009**, *31*, 330.
[19] R. Gref, P. Couvreur, G. Barratt, E. Mysiakine, *Biomaterials* **2003**, *24*, 4529.
[20] P. Zhao, H. Wang, M. Yu, Z. Liao, X. Wang, F. Zhan, W. Ji, B. Wu, J. Han, H. Zhang, H. Wang, J. Chang, R. Niu, *Eur. J. Pharm. Biopharm.* **2012**, *81*, 248.
[21] A. Rungta, B. Natarajan, T. Neely, D. Dukes, L. S. Schadler, B. C. Benicewicz, *Macromolecules* **2012**, *45*, 9303.
[22] S. Maslanka Figueroa, A. Veser, K. Abstiens, D. Fleischmann, S. Beck, A. Goepferich, *Proc. Natl. Acad. Sci. USA* **2019**, *116*, 9831.
[23] Z. L. Yang, X. R. Li, K. W. Yang, Y. Liu, *J. Biomed. Mater. Res., Part A* **2008**, *85A*, 539.
[24] S. Bosnyak, E. S. Jones, A. Christopoulos, M.-I. Aguilar, W. G. Thomas, R. E. Widdop, *Clin. Sci.* **2011**, *121*, 297.
[25] M. de Gasparo, K. J. Catt, T. Inagami, J. W. Wright, T. Unger, *Pharmacol. Rev.* **2000**, *52*, 415.
[26] D. Coates, *Int. J. Biochem. Cell Biol.* **2003**, *35*, 769.
[27] W. Jiang, B. Y. S. Kim, J. T. Rutka, W. C. W. Chan, *Nat. Nanotechnol.* **2008**, *3*, 145.
[28] R. Hennig, K. Pollinger, J. Tessmar, A. Goepferich, *J. Drug Targeting* **2015**, *23*, 681.
[29] B. J. Ballermann, K. L. Skorecki, B. M. Brenner, *Am. J. Physiol.* **1984**, *247*, F110.
[30] P. G. de Gennes, *Adv. Colloid Interface Sci.* **1987**, *27*, 189.
[31] N. Dos Santos, C. Allen, A.-M. Doppen, M. Anantha, K. A. K. Cox, R. C. Gallagher, G. Karlsson, K. Edwards, G. Kenner, L. Samuels, M. S. Webb, M. B. Bally, *Biochim. Biophys. Acta, Biomembr.* **2007**, *1768*, 1367.
[32] K. Abe, K. Higashi, K. Watabe, A. Kobayashi, W. Limwikrant, K. Yamamoto, K. Moribe, *Colloids Surf. A* **2015**, *474*, 63.
[33] S. Wang, E. E. Dormidontova, *Phys. Rev. Lett.* **2012**, *109*, 238102.
[34] R. Eisenthal, M. J. Danson, D. W. Hough, *Trends Biotechnol.* **2007**, *25*, 247.
[35] S. J. York, L. S. Arneson, W. T. Gregory, N. M. Dahms, S. Kornfeld, *J. Biol. Chem.* **1999**, *274*, 1164.
[36] Z. Poon, S. Chen, A. C. Engler, H. Lee, E. Atas, G. von Maltzahn, S. N. Bhatia, P. T. Hammond, *Angew. Chem., Int. Ed.* **2010**, *49*, 7266.

[37] Q. Dai, C. Walkey, W. C. W. Chan, *Angew. Chem., Int. Ed.* **2014**, *53*, 5093.
[38] Q. Dai, S. Wilhelm, D. Ding, A. M. Syed, S. Sindhwani, Y. Zhang, || Yih, Y. Chen, P. Macmillan, W. C. W. Chan, *ACS Nano* **2018**, *12*, 8423.
[39] E. Boucrot, S. Saffarian, R. Massol, T. Kirchhausen, M. Ehrlich, *Exp. Cell Res.* **2006**, *312*, 4036.
[40] H. Liu, Y. Liu, S. Liu, D.-W. Pang, G. Xiao, *J. Virol.* **2011**, *85*, 6252.
[41] H. P. Erickson, *Biol. Proced. Online* **2009**, *11*, 32.
[42] Homo sapiens type-1 angiotensin II receptor – Protein – NCBI, https://www.ncbi.nlm.nih.gov/protein/?term=Homo+sapiens+type-1+angiotensin+II+receptor (accessed: February 2019)
[43] B. Baudin, P. A. Timmins, L. Drouet, Y. Legrand, F. C. Baumann, *Biochem. Biophys. Res. Commun.* **1988**, *154*, 1144.
[44] N. T. Huynh, E. Roger, N. Lautram, J.-P. Benoît, C. Passirani, *Nanomedicine* **2010**, *5*, 1415.
[45] H. Qian, A. R. Wohl, J. T. Crow, C. W. Macosko, T. R. Hoye, *Macromolecules* **2011**, *44*, 7132.
[46] K. Abstiens, S. Maslanka Figueroa, M. Gregoritza, A. M. Goepferich, *Soft Matter* **2019**, *15*, 709.
[47] C. E. Childs, *Microchem. J.* **1975**, *20*, 190.
[48] J.-M. Rabanel, J. Faivre, S. F. Tehrani, A. Lalloz, P. Hildgen, X. Banquy, *ACS Appl. Mater. Interfaces* **2015**, *7*, 10374.
[49] G. Grynkiewicz, M. Poenie, R. Y. Tsien, *J. Biol. Chem.* **1385**, *260*, 3440.
[50] V. B. Damodaran, C. J. Fee, T. Ruckh, K. C. Popat, *Langmuir* **2010**, *26*, 7299.